CHAPTER 2 THEORY AND LITERATURE REVIEW

This research was focussed on the development of the synthetic methods and characterisation (structural, thermal, magnetic and redox properties) of two types of ionic copper(II) mixed carboxylates: (a) $K_a[Cu_2(p\text{-}OC_6H_4COO)_a(CH_3(CH_2)_nCOO)_{4-a}]$, and (b) $[Cu_2(p\text{-}H_3NC_6H_4COO)_a(CH_3(CH_2)_{14}COO)_{4-a}]X_a$, where $a = 1, 2$; $n = 14, 10, 8$, and 6; $X = Cl, CH_3COO$ and CF_3SO_3. These complexes were designed to be thermally stable and magnetic metallomesogens and/or metal-containing ionic liquids. The latter complexes were also designed to function as solvent-cum-catalysts in the carbon-carbon bond-forming reaction of carbonyls. Accordingly, this chapter presents the relevant theories and literature review related to this research.

2.1 Metallomesogens

Metallomesogens are also known as metal-containing liquid crystals [1-3]. These materials combine the properties of liquid crystals (such as anisotropy and fluidity) with those of metals (such as colour, magnetism, polarizability, multiple localized charges, and variable geometries), which leads to the formation of mesophases which are unobtainable in organic liquid crystals [1].

The liquid crystal state (termed mesophase) exists between the solid and liquid states. Molecules (mesogens) of liquid crystals have the tendency to point along a common axis (known as director). Hence, they contrast with molecules in the liquid phase (which do not have intrinsic order) and in the solid state (which are highly ordered with little translational freedom). **Figure 2.1** shows the different arrangement of molecules for each state.

(a)   (b)   (c)
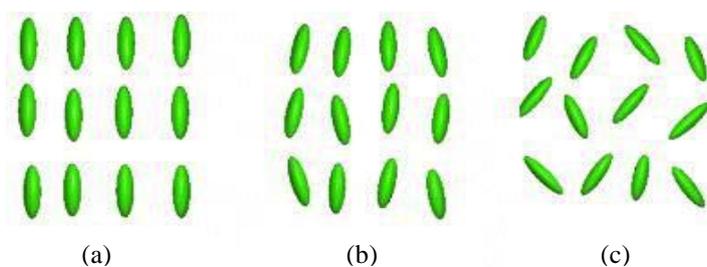
Figure 2.1 Different molecular arrangement in (a) solid; (b) liquid crystal; and (c) liquid

Liquid crystals may be divided into two categories depending on how the mesophase is formed: (a) thermotropic (temperature dependent). Most metallomesogens are of this type); and (b) lyotropic (concentration and solvent dependent).

Thermotropic liquid crystals are made up of a central rigid core (for example, an aromatic ring) and a flexible peripheral moiety (generally aliphatic groups). It can be classified into two general classes: (a) calamitic or rod-like (possess elongated shape); and (b) discotic or disc-like. Calamitic liquid crystals may exhibit two common types of mesophases, namely nematic (N) and smectic (S).

The N phase is the least ordered mesophase (the closest to the isotropic liquid state), where the molecules have only an orientational order (**Figure 2.2).**
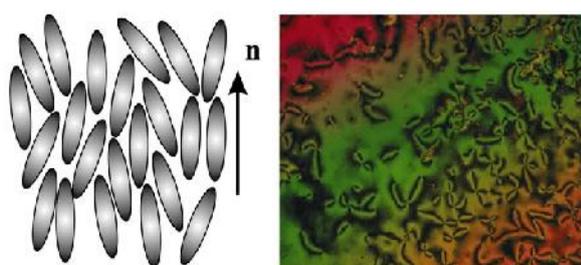

Figure 2.2 The nematic phase: (left) an illustration of the orientation of the molecules, and (right) an optical micrograph of the characteristic Schlieren texture

The S phase posseses both an orientational and positional orders (layered structures), and can be devided into many subclasses, such as smectic A (S_A), where the layers are perpendicular to the director, and smectic C (S_C), when the director is tilted at an angle to the normal (the *z axis*). Both phases are shown in **Figure 2.3**.
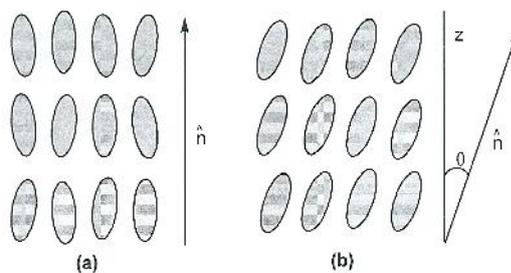
Figure 2.3 A molecular arrangement of: (a) S_A phase; and (b) S_C phase

Examples of S_A and Sc phases are shown in **Figure 2.4** and **Figure 2.5** respectively.
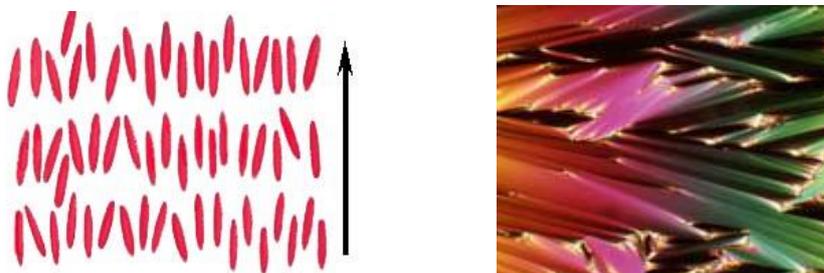
Figure 2.4 An illustration of smectic A phase *(left)*, and the optical texture of the phase viewed under a polarizing microscope *(right)*
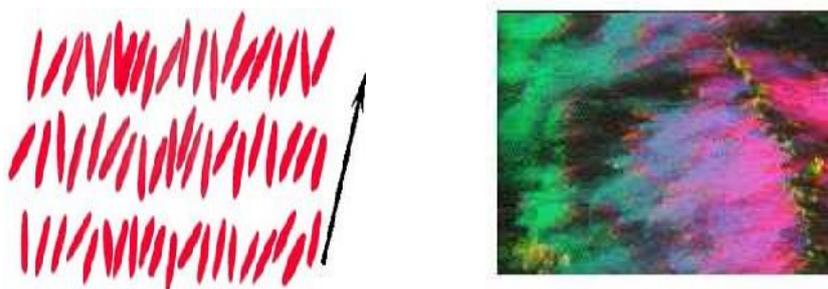

Figure 2.5 An illustration of smectic C phase (*left*) and the optical texture of the phase viewed under a polarizing microscope (*right*)

Many calamitic systems are based on transition metals, which are capable of forming complexes with a square planar or linear geometry. **Figure 2.6** shows two examples of these metallomesogens [4,5].
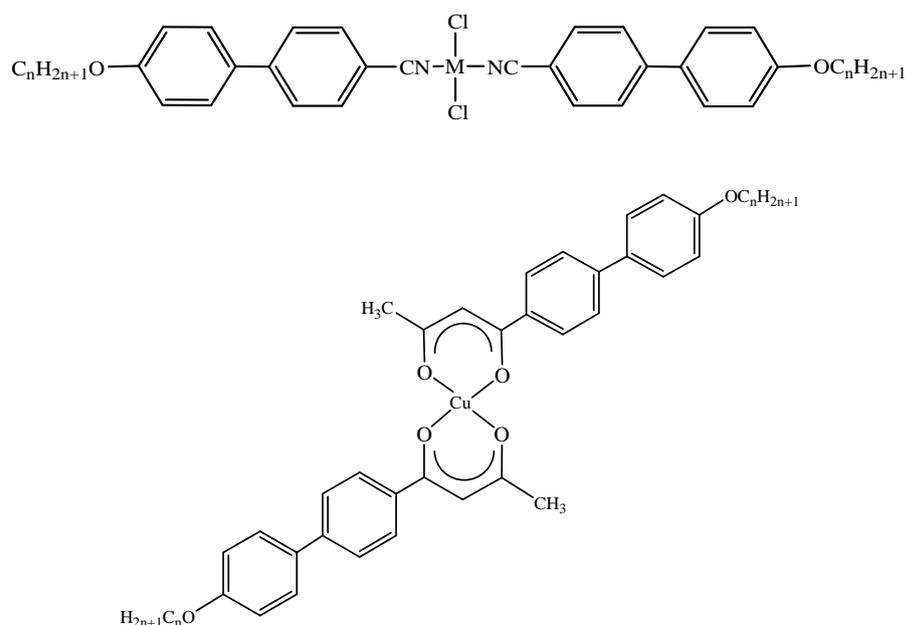
Figure 2.6 Examples of calamitic metallomesogens

The general structure of discotic (disc-shape) liquid crystals comprises of a planar (usually aromatic) central rigid core surrounded by usually four, six or eight flexible peripheries (mostly pendant chain). Hexa-substituted benzene derivatives **(Figure 2.7)**, synthesized by Chandrasekhar *et al*. [6] are the first series of organic discotic compounds to exhibit mesophases.
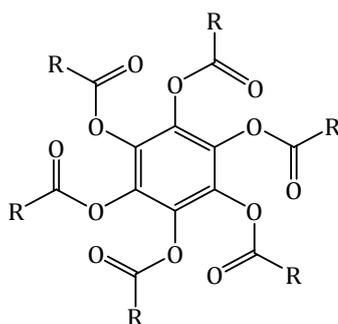
Figure 2.7 Molecular structure of the first series of discotic liquid crystals discovered: benzene-hexa-*n*-alkanoate derivatives (R = C_4H_9 to C_9H_{19})

Discotic liquid crystals exhibit two main types of mesophases with varying degree of organisation, namely nematic discotic (N_D) and columnar (Col).

The N_D phase is the least ordered mesophase as the molecules have only orientational order (no positional order), as illustrated in **Figure 2.8**.
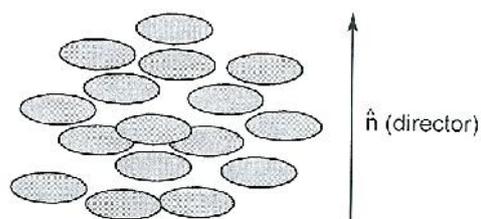
Figure 2.8 An illustration of a molecular arrangement of N_D phase

The Col phase is more ordered and has a tendency to stack one on top of another, to form columns with different lattice patterns. As a results, a number of columnar mesophases are identified, such as columnar rectangular (Col$_r$) and columnar hexagonal (Col$_h$). These are illustrated in **Figure 2.9**.
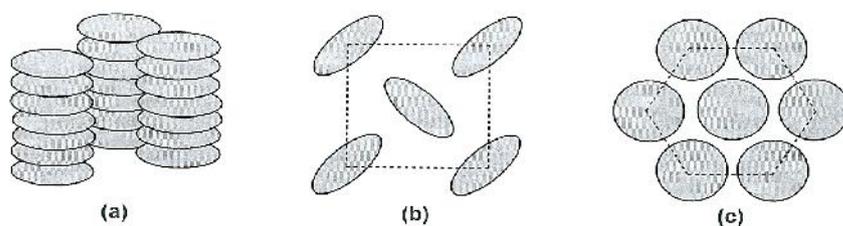

Figure 2.9 (a) The general structure of Col phases; (b) a representation of Col$_r$; and (c) a representation of Col$_h$

Copper complexes of -diketonates **(Figure 2.10)**, which possess a square planar geometry, are good examples of discotic metallomesogens [1].
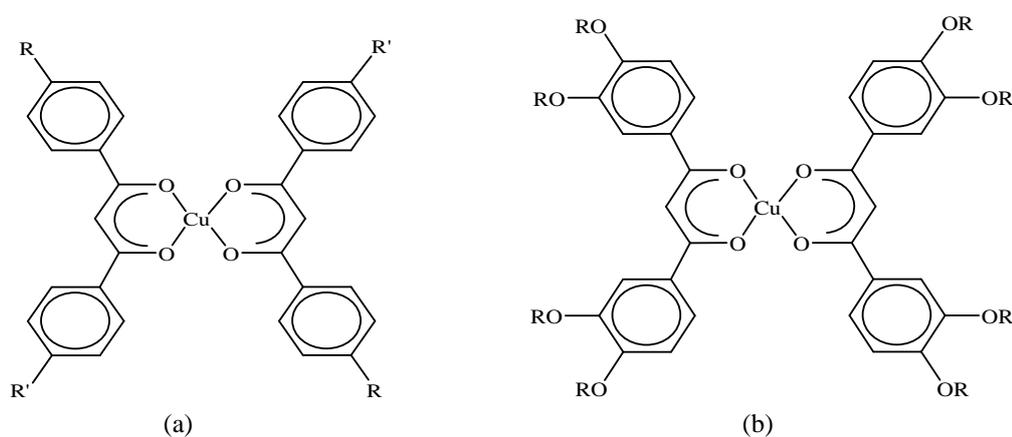

Figure 2.10 Examples of discotic metallomesogens: (a) four-chain -diketonates, and (b) eight-chain -diketonates

Among the various metallomesogens already explored, binuclear carboxylates of divalent transition metals, of general formula $[M_2(RCOO)_4]$ where M = Cu(II), Rh(II), Ru(II), Mo(II), and Cr(II), have been widely studied [7]. It is to be noted that all binuclear carboxylates of this class exhibit the so-called 'lantern' or 'paddle-wheel' structure, exemplified by $[Cu_2(CH_3COO)_4(H_2O)_2]$ (**Figure 2.11**) [8].
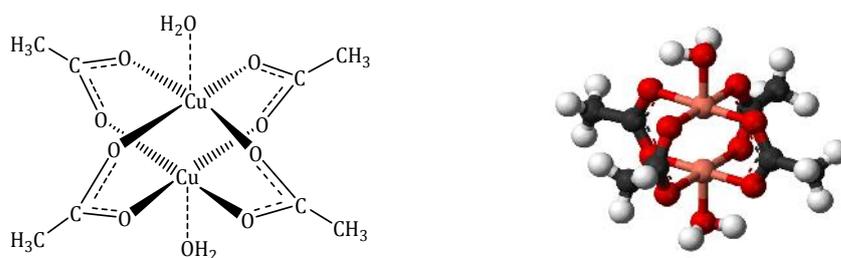
Figure 2.11 Lantern or paddle-wheel structure of $[Cu_2(CH_3COO)_4(H_2O)_2]$

Copper(II) salts of straight chain aliphatic carboxylates consist of columnar stacks of dimers and hence showed discotic mesophases. **Figure 2.12** shows the stacking of these discotic molecules [9].

(a)   (b)
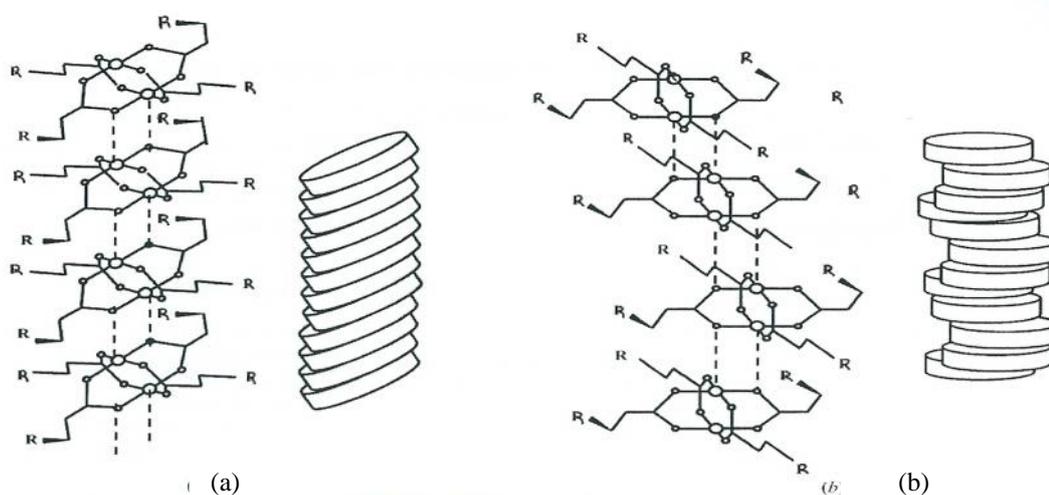
Figure 2.12 Lantern or paddle wheel structure of the dicopper(II) tetraalkanoate, stacking in the two possible ways for the formation of the columnar phase: (a) tilted to the columnar axis for the tetragonal phase; and (b) parallel to the columnar axis for the hexagonal phase

2.2   Metal-Containing Ionic Liquids

Ionic liquids (ILs) are defined as salts that melt at or below $100^{o}C$ [10]. Ionic liquids that are free-flowing at room temperature are called ambient temperature ionic liquids.

The initial interests in ILs arises mainly because of their possible use as 'greener' alternatives to volatile organic solvents. This is because these materials have relatively low viscosities and exhibit very low vapour pressure under ambient conditions [10]. However, currently ionic liquids have other important uses, such shown in **Figure 2.13**.
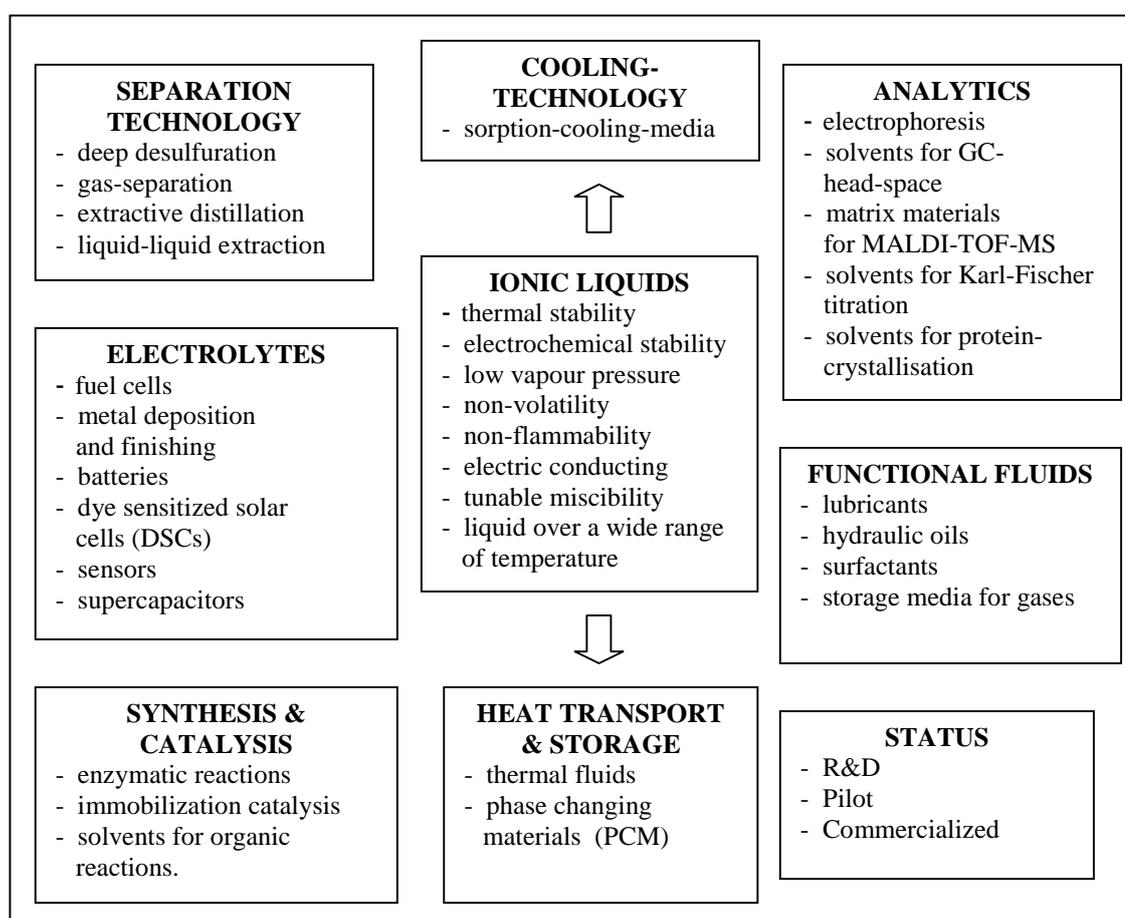
Figure 2.13 Applications of ionic liquids

Currently, most research on ionic liquids are based on cations, namely imidazolium, ammonium and pyridinium (known as nitrogen-based ILs), and on phosphonium cores (**Figure 2.14).**
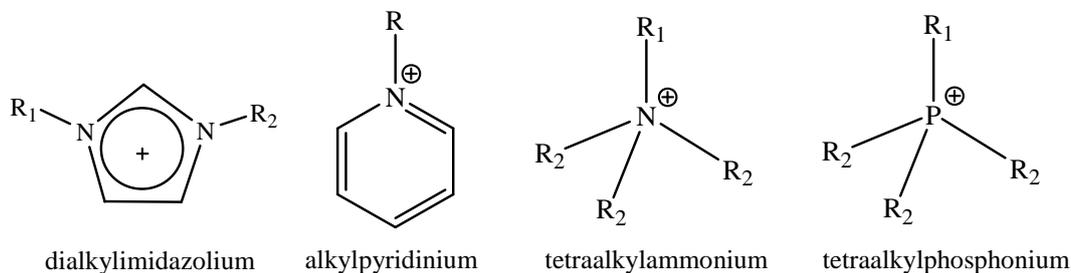
Figure 2.14 Examples of cations of ionic liquids

The anions are mainly inorganic species, such as $[BF_4^-]$, $[PF_6^-]$, $[X^-]$, $[NO_3^-]$, $[OH^-]$, $[CN^-]$, and halometallates $[MX_n^{m-}]$, where X is an halide. Examples of organic anions are $[RCOO^-]$ and $[CF_3SO_3^-]$ [10].

Metal-containing ionic liquids (MetILs) **(Figure 2.15)** are a large class of highly modifiable molten salts [11]. They offer the possibility of more highly charged species (for example, $[LnX_6^{3-}]$) and additional variations in geometries (examples, tetrahedral and square planar $[MX_4^{2-}]$) [12].
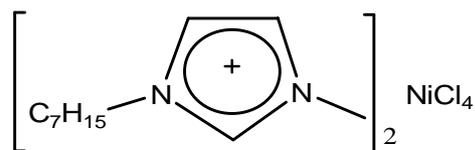
Figure 2.15 An example of a metal-containing ionic liquid [12]

The important characteristics of metal-containing ionic liquids are high thermal stability, negligible vapour pressure, wide electrochemical window and the ability to dissolve a range of organic and inorganic compounds. These have been exploited in the context of separations, catalysis and electrochemistry [11].

2.3 Copper(II) Carboxylates

The chemistry of copper(II) complexes has received a great deal of attention in several different fields, ranging from catalysis to bioinorganic and material chemistry. Copper is a transition metal with the electronic configuration $[Ar]3d^{10}4s^1$. It commonly forms complexes as Cu^+ ($3d^{10}$) or Cu^{2+} ($3d^9$) ions, and in some rare cases, as Cu^{3+} ($3d^8$) ion. Cu^{2+} is the most stable and important ion for copper and plays a crucial role in several characterization methods of the complexes formed, such as electronic spectroscopy, magnetic susceptibility and electron paramagnetic resonance spectroscopy [13].

Copper(II) carboxylates are made up of central copper(II) bonded to a fix numbers of carboxylate ions (oxygen donor ligands), by coordinated covalent bonds [14]. Carboxylate anions are versatile ligands because each of its oxygen atom carries two lone pairs. Various coordination modes are thus possible [15] (**Figure 2.18**; shown later). It is noted that diverse structures of these complexes have been reported, such as mononuclear, binuclear and polynuclear [13].

However, most copper(II) carboxylates have the dinuclear paddle-wheel structure (**Figure 2.11**). This is the structure adopted by copper(II) acetate [8], and the structure suggested for other copper(II) carboxylates, such as copper(II) butanoate, copper(II) hexanoate, copper(II) octanoate and copper(II) decanoate [9]. The structure consists of a dimer made up of two copper(II) ions bonded to four bridging bidentate carboxylates. As such, there is a significant electronic and magnetic communications between the two unpaired electrons on the copper(II) centres, and allows ready delocalization of electrons [16].

In the dinuclear paddle-wheel structure, only one of the lone pairs of each oxygen atom is involved in coordination. However, stepped polymeric structure may also form (**Figure 2.16**) [15].
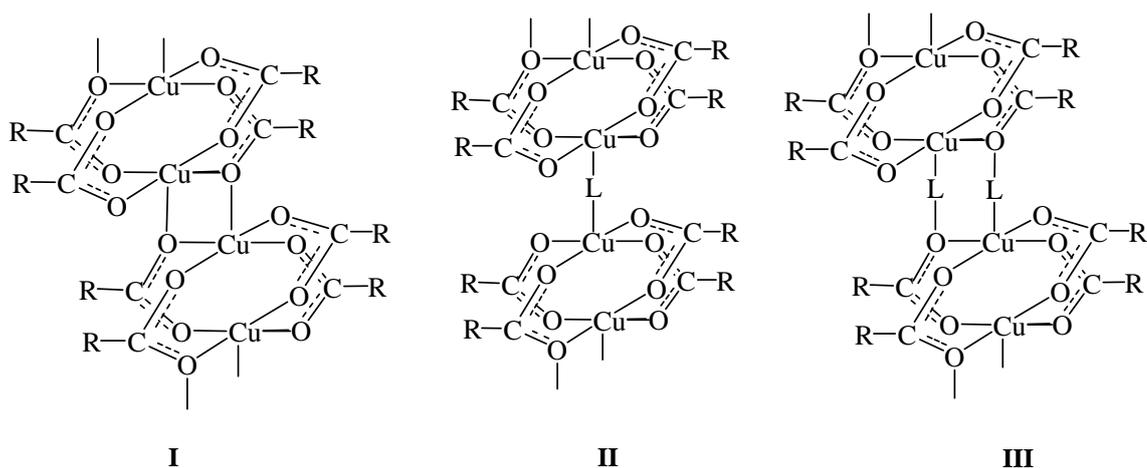
Figure 2.16 General structure of polynuclear copper(II) carboxylates: (**I**) stepped without additional ligands; (**II**) ligands bridging two Cu; and (**III**) ligands bridging Cu and O

2.4 The C-C Bond-Forming Reactions

The formation of a carbon-carbon bond is very important to the success of synthetic organic chemistry. An example is the aldol reaction of carbonyls (aldehydes and ketones), proposed to proceed by two different mechanisms: (a) enol; and (b) enolate mechanisms.

In the enol mechanism, the carbonyl compounds are converted to enols or enol ethers. These compounds, being nucleophilic at the -carbon, can attack especially reactive protonated carbonyls [17].

In the enolate mechanism, the carbonyl compounds, being carbonic acids, are deprotonated to form enolates, which are much more nucleophilic than enols or enol ethers, and therefore can attack electrophiles directly. The usual electrophile is an aldehyde, since ketones are much less reactive. Both enol and enolate mechanisms are shown in **Figure 2.17** [17].
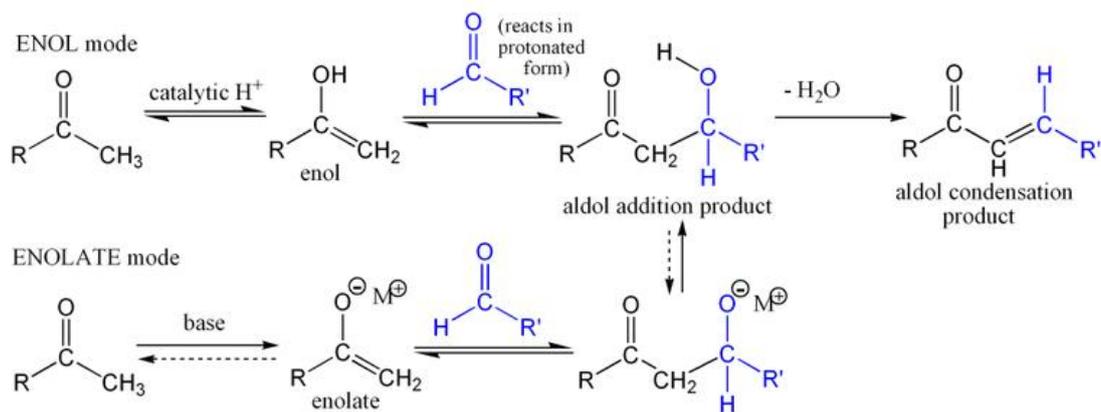
Figure 2.17 The enol (top) and enolate (bottom) mechanisms of aldol condensation of carbonyl compounds

Recently, it was accidentally discovered that copper(II) arylcarboxylates reacted with acetone in the presence of HCl, to form black solids [18]. These solids were soluble in most organic solvents, insoluble in water, have physical characteristic tuned by the arylcarboxylates used, were redox active, and thus potential low band-gap photonic materials and redox catalysts. One of the component of these solids were a product formed in the C-C bond forming product of acetone molecules. Thus, this reaction would serve as a new and facile synthetic method for such industrially important organic products.

2.5 Elemental Analyses

Elemental analyses is the determination of the mass fractions of carbon, hydrogen, nitrogen, and heteroatoms (X) (halogens, sulfur) of a sample. The results helps in the determination of the chemical formula of an unknown substance.

CHN analysis is the most common form of elemental analyses. The technique used involves combustion; a sample is burned in an excess of oxygen, and the products of the combustion, carbon dioxide, water, and nitric oxides, are collected by various traps. The masses of these combustion products may be used to calculate the percentage

composition of the unknown sample, and then the empirical formula (the simplest whole-number ratios of the elements) [19].

2.6 Fourier Transform Infrared Spectroscopy

Fourier transform infrared spectroscopy (FTIR) is an important tool to identify functional groups and types of chemical bonds in a molecule. It involved infrared radiation between 4000 cm^{-1} to 400 cm^{-1} (between the visible and microwave regions in the electromagnetic spectrum).

It is based on the principle that almost all molecules absorb infrared light only at certain frequencies, where it affects the dipolar moment of the molecule. The data is collected and converted from an interference pattern to the absorption spectrum which provides a unique characteristic for each molecule.

For metal carboxylates, FTIR spectra are additional useful as it may be used to determine the coordination mode of the carboxylate ligands. In metal complexes, a carboxylate ion, RCOO^{-}, can coordinate to metals mainly as monodentate, chelating or bridging bidentate (*syn-syn*, *syn-anti* or *anti-anti* configuration) ligands (**Figure 2.18**).

Figure 2.18 Coordination of carboxylate ligand: (I) monodentate; (II) chelating; amd (III) bridging bidentate: (a) *syn-syn,* (b) *syn-anti,* (c) *anti-anti*

The type of binding mode is deduced from the Δ value (the separation between the two carboxylate stretching modes, $\nu(COO)_{asym}$ and $\nu(COO)_{sym}$). The Δ values of greater than 200 cm^{-1} indicate a monodentate coordination [21], those between 120 cm^{-1} to 180 cm^{-1} indicate a bridging coordination [22,31], while those lower than 120 cm^{-1} indicate a chelating coordination. The assessment of the relationship was initially based on the infrared data of acetato and trifluoroacetato complexes, which were later extended to other alkyl or aryl carboxylate ions [20].

2.7   UV-Visible Spectroscopy

UV-vis spectroscopy involves measurements of light absorbed at wavelength within the ultraviolet (200-400 nm), visible (400-700 nm) and near infrared (700-1000 nm) regions of the electromagnetic spectrum. The energies within these wavelengths are sufficient to excite an electron to higher energy orbitals.

Most transition metal complexes are coloured due to the electronic transitions (either *d-d* or charge transfer). A *d-d* transition involves the excitation of an electron in a *d* orbital of a metal by a photon of visible light, to another higher energy *d* orbital (the excited state). Only light with wavelengths (λ) that exactly match the energy difference between the ground and the excited states will be absorbed. When this happens, the light that is not absorbed is transmitted, and gives the colour of the complex (which is on the opposite side of the colour that is absorbed – refer to the colour wheel, **Figure 2.19).** For example, a substance that absorbs light of wavelength 600-620 nm appears blue, while that that absorps at 680-700 nm appears green.
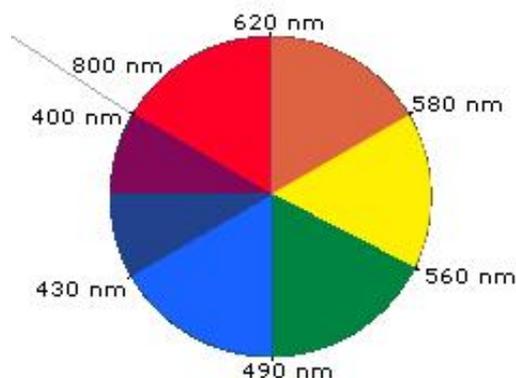
Figure 2.19 The colour wheel

A charge transfer band is due to the excitation of an electron, either from a metal-based orbital into an empty ligand-based orbital (known as metal-to-ligand charge transfer - MLCT), or from a ligand-based orbital into an empty metal-based orbital (known as ligand-to-metal charge transfer - LMCT).

When UV-visible radiation is passed through a solution contained in a cell of path length, l, some of the radiation is absorbed while others is transmitted. The transmitted radiation has a certain intensity, I. If only the solvent is contained in the cell, the transmitted radiations has an intensity, I_o. The ratio of I to I_o is known as transmittance, T of the sample. The relationship is:

$$T = I/I_o$$

An exponential curve is obtained when T is plotted against l. A linear graph is obtained when a logarithmic function of T is used. Absorbance, A, which is the amount of light absorbed by substance, is defined as:

$$A = \log (1/T) = \log I_o/I$$

where A is the absorbance.

The relationship between the absorbance, concentration and path length is known as Beer-Lambert's law:

$$A = \varepsilon cl$$

where ε is the molar absorptivity, c is the concentration in mol dm^{-3} and l is the path length in cm. A recording of A as a function of the wavelength produces the absorbance spectrum.

The UV-vis absorption spectra are very useful in providing information on the geometry of metal complexes, deduce from the wavelength of the d-d band (λ_{max}, wavelength of absorption maxima). For copper(II) complexes, the expected λ_{max} for a tetrahedral complex is normally at about 800 nm, a square pyramidal complex at about 700 nm [23,24], and a square planar complex at about 600 nm [25].

The crystal-field theory (CFT) can be used to explain the electronic structure of metal complexes. This is done by determining the energy changes of five degenerate d orbitals **(Figure 2.20)** when surrounded by ligands (illustrated as an array of point charges).
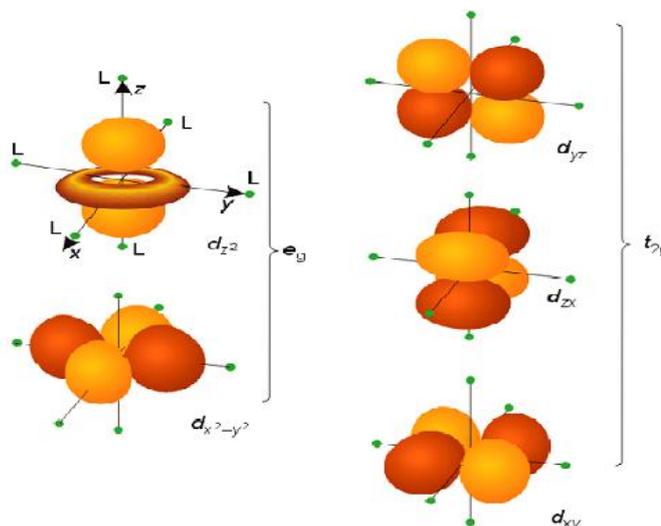

Figure 2.20 Shapes (angular dependence functions) of the d orbitals

As a ligand approaches the metal ion, the electrons in the d orbitals and in the ligand experiences repulsion. As a result, the d electrons closer to the ligands will have higher energy than those further away. Thus, the five d orbitals loss its degeneracy. The

splittings of the *d* orbitals for tetrahedral, octahedral, and square planar complexes are shown in **Figure 2.21.**
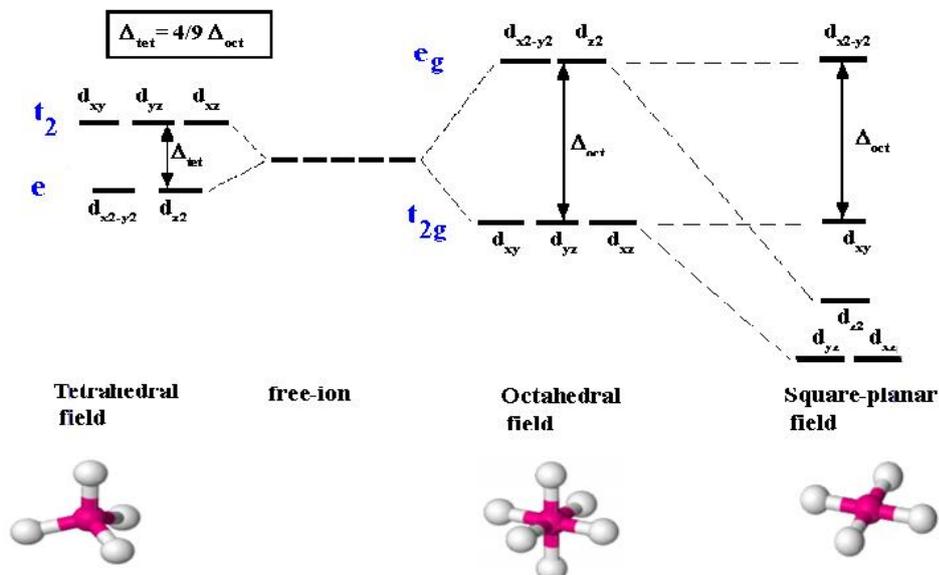

Figure 2.21 Splitting of *d* orbitals for tetrahedral, octahedral and square planar complexes

An octahedral complex has six ligands, forming an octahedron around the metal ion. In this situation, the *d* orbitals split into two sets: two higher-energy orbitals, termed e_g (d_z^2 and $d_{x^2-y^2}$), and three lower-energy orbitals, termed t_{2g} (d_{xy}, d_{xz} and d_{yz}). The energy difference, $_{oct,}$ is known as the crystal-field splitting parameter.

A tetrahedral complex has four ligands, forming a tetrahedron around the metal ion. The energy splitting is the opposite of that of an octahedral complex. The *d* orbitals split into three higher energy orbitals, termed t_2 (d_{xy}, d_{xz} and d_{yz}), and two lower energy orbitals, termed *e* (d_z^2 and $d_{x^2-y^2}$). The energy difference is $_{tet}$, which is lower (about $^4/_9$ $_{oct}$). This is because there are only four ligands and that the ligand electrons are not oriented directly towards the *d* orbitals.

Many complexes experience geometrical distortion. This is explained by the Jahn-Teller theorem, published in 1937, which states that "*any non-linear molecular system*

in a degenerate electronic state will be unstable and will undergo distortion to form a system of lower symmetry and lower energy, thereby removing the degeneracy" [26].

For copper(II) complexes(d^9 configuration), the $d_z{}^2$ and $d_x{}^2{}_{-y}{}^2$ orbitals are unequally occupied. To minimize repulsion with the ligands, two electrons occupy the $d_z{}^2$ orbital and one electron occupy the $d_x{}^2{}_{-y}{}^2$ orbital. Consequently, there is a stronger repulsion along the z-axis. Hence, most copper(II) complexes have an elongation along the z-axis, which leads to square planar geometry.

Similarly, CFT can be used to explain the splitting of d orbitals for other geometries. This is shown in **Figure 2.22**.
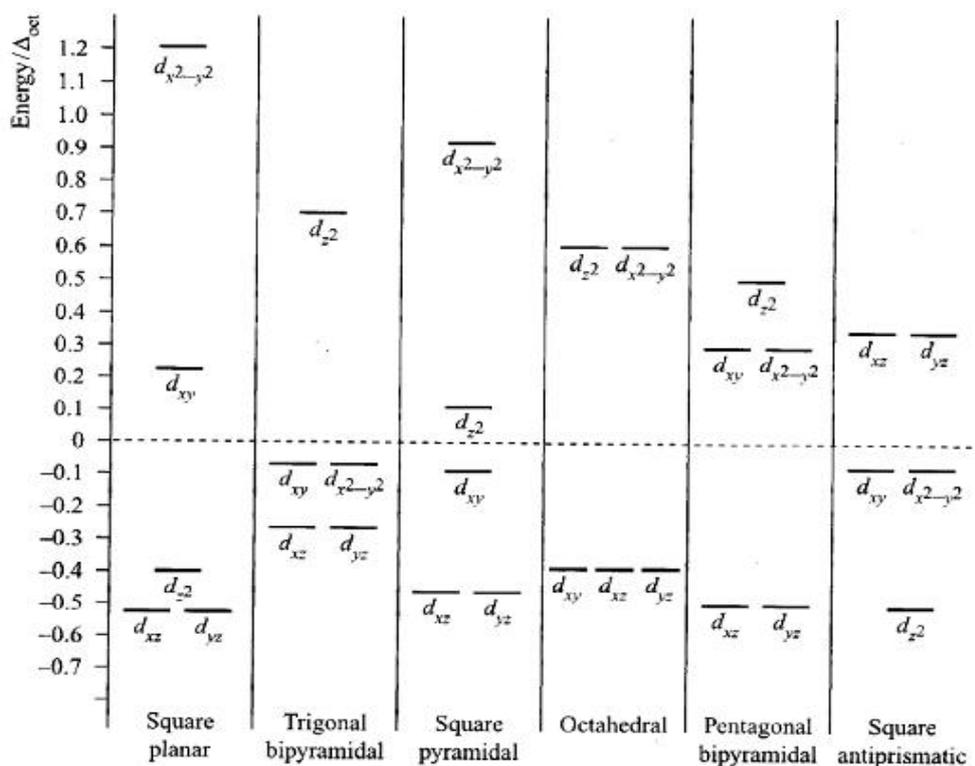

Figure 2.22 Crystal-field splitting of d orbitals for complexes of various geometry

UV-vis spectroscopy also provides useful information on the nuclearity of complexes, deduced from the values of molar absorptivity ($_{max}$). This value measures the strength of the light absorbed by a chromophore at a given wavelength. For most

mononuclear copper(II) complexes, the values of $_{max}$ are about 100 M^{-1} cm^{-1} [27,28]. Hence a value of greater than 200 $M^{-1}cm^{-1}$ suggests two Cu(II) chromophores [29].

2.8   Thermal Analyses

Thermal analyses involve the study of properties of materials with changes of temperature. Two examples are thermogravimetry and differential scanning calorimetry.

2.8.1 Thermogravimetric Analysis

Thermogravimetric analysis (TGA) measures the amount of weight loss (in %) of a sample as a function of temperature in a controlled atmosphere (inert gas, N_2) up to 900^oC.

The analyzer consists of a high-precision balance with a pan loaded with the sample, placed in a small oven with a thermocouple (electrically heated), to measure the temperature accurately. To control the instrument, a computer is connected to the analyzer.

The results are displayed as a TGA curve (thermogram) in which weight % is plotted against temperature. It is used to determine the thermal stability, the decomposition process and the amount of residue left at the end of the experiment.

As an example, the thermogram of a sample of copper(II) benzoate, $[Cu_2(C_6H_5COO)_4(CH_3CH_2OH)_2]$ is shown in **Figure 2.23** [16]. It shows that the sample was thermally stable up to around 230^oC. It then decomposed in a two-step process. The initial weight loss of 7.4% at 81.7^oC is assigned to the loss of CH_3CH_2OH at the axial positions (expected 9.7%). The total weight loss of 68.3% (expected 68.8%) is assigned to the decomposition of the carboxylates ligands to CO_2 and other volatiles.

For many copper(II) carboxylates, it has been suggested that the residue is mainly copper(II) oxide [23,30]. By using the gravimetry concept, the formula mass of metal

complexes may be calculated. Thus, the TGA can be an alternative technique used to support the proposed structure of a complex, in the absence of crystal data.
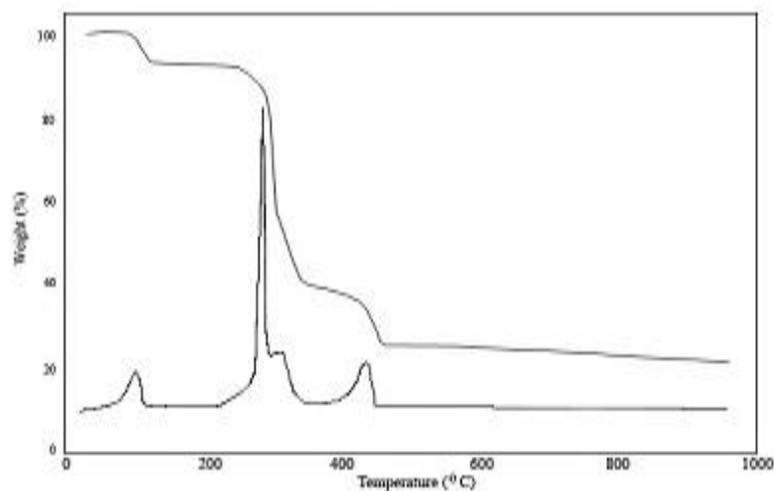

Figure 2.23 TG and DTA curves of [$Cu_2(C_6H_5COO)_4(C_2H_5OH)_2$]

2.8.2   Differential Scanning Calorimetry

Differential scanning calorimetry (DSC) is used mainly in studying the phase transitions, such as fusion and crystallization, glass transition, melting and clearing temperatures **(Figure 2.24)**. During the phase transition, more or less heat will flow to the sample than the reference (an inert material such as empty aluminium pan), to maintain both at the same temperature. It depends on whether the process is endothermic (heat is absorbed, such as melting and glass transition), or exothermic (heat is released, such as crystallization and formation of a chemical bond).
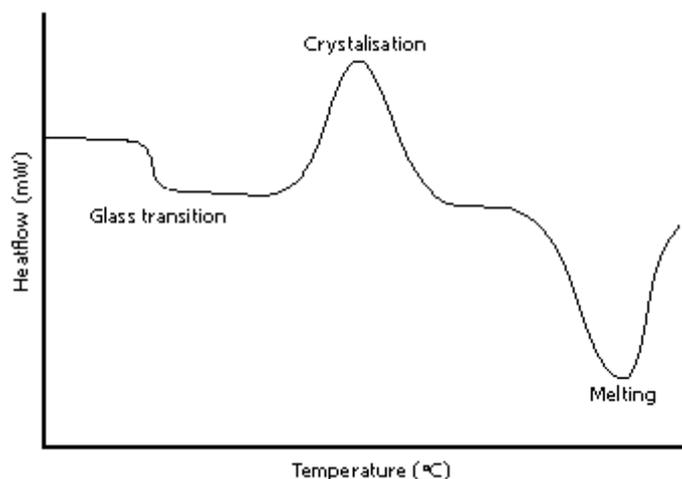
Figure 2.24 An example of a DSC curve

The amount of heat absorbed or released is measured, and the result is recorded as a curve of heat flow versus temperature. It is then used to calculate enthalpies of transitions (H). The reaction is either endothermic (H = positive) or exothermic (H = negative).

2.9 Optical Polarizing Microscopy

Optical polarising microscopy (OPM) is useful in providing information on the phase transition and the study of mesomorphism of liquid crystals. It is designed to observe and photograph samples that are visible due to their optically anisotropy.

For the identification of the liquid crystalline mesophases, the texture observed by is analyzed and compared with published results. Some examples of liquid crystal phase textures are shown in **Figure 2.25** [32].

(a)　　　　　　　　　　　　(b)　　　　　　　　　　　　(c)

(d)　　　　　　　　　　　　(e)　　　　　　　　　　　　(f)
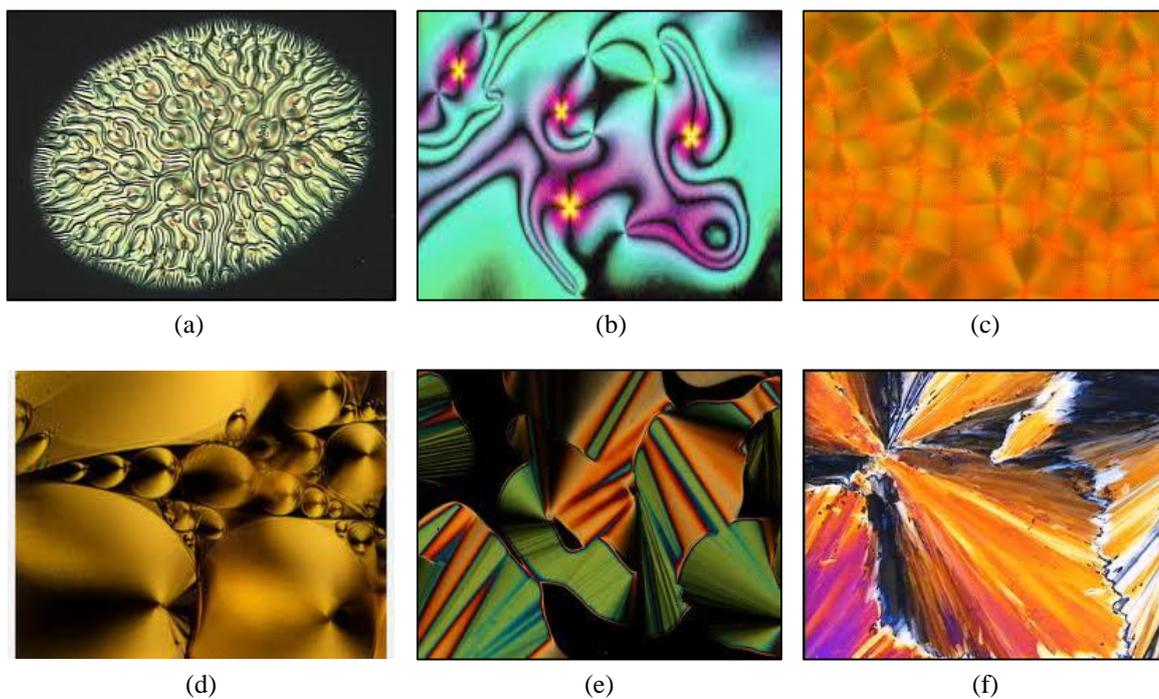
Figure 2.25 OPM textures of different phases of liquid crystals: (a) N droplets; (b) N; (c) cholesteric; (d) S_A ; (e) D_h; and (f) spherulite texture of a crystalline phase

For copper(II) linear alkylcarboxylates with 4 to 21 carbon atoms, a phase transition from lamellar crystalline solid to a hexagonal liquid-crystalline phase is observed [33] **(Figure 2.26)**.
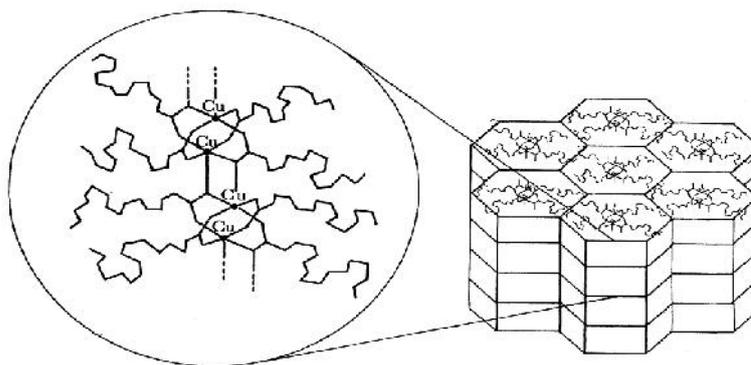

Figure 2.26 A schematic view of the columnar mesophase of copper(II) linear alkylcarboxylates. Each column is made of stacked dicopper tetracarboxylate units.

For example, the optical structure of copper(II) butanoate showed a homeotropic tetragonal, while copper(II) pentanoate and copper(II) hexanoate showed hexagonal columnar discotic mesophases (**Figure 2.27**) [9].


| (a) | (b) | (c) |

| (d) | (e) | (f) |
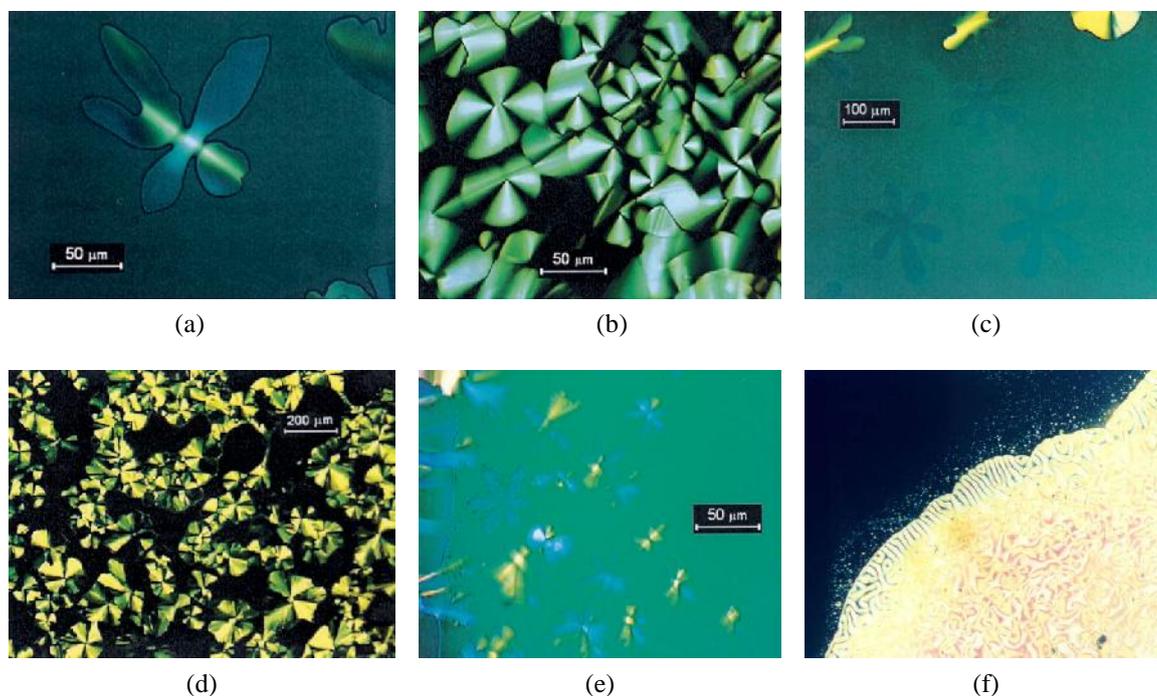
Figure 2.27 OPM of (a) copper(II) butanoate showing (a) tetragonal domains at 184.1^{o}C; (b) copper(II) butanoate showing typical columnar developable domains at 164.7^{o}C; (c) copper(II) pentanoate showing hexagonal homeotropic domains at 98.9^{o}C; (d) copper(II) pentanoate showing developable domains at 118.9^{o}C; (e) copper(II) hexanoate showing hexagonal homeotropic domains at 135°C; and (f) copper(II) hexanoate showing developable domains for copper(II) hexanoate at 152°C

OPM and DSC are used together to give useful information on the phase transitions of liquid crystals. As an example, the DSC of [Cu$_2$(RCOO)$_4$], where R = CH$_3$(CH$_2$)$_n$, n = 12, 14, 16 and 18, shows an endotherm at 105-117°C [31], which may be assigned as a phase transition from solid state (crystal state), liquid-crystal state or thermotropic column mesophase.

2.10 Magnetic Susceptibility

Magnetic properties of materials are studied by applying a magnetic field and measuring the induced megnetization. Some materials are repelled (diamagnetism), others are attracted to a magnetic field (paramagnetism).

Diamagnetic materials have no net magnetic moments because they do not have unpaired electrons. The magnetic fields are produced from the tiny current loops created by orbital motions of the electrons. When an external magnetic field is applied, these current loops are aligned to oppose the applied field producing a negative magnetization and thus negative susceptibility.

Paramagnetic materials have permanent magnetic moments (dipoles) due to the spin of unpaired electrons. When a magnetic field is applied, the dipoles are aligned in the same direction of the applied field, resulting in a net positive magnetic moment and positive susceptibility.

In the absence of an external field, the dipoles do not interact with one another and are randomly oriented due to thermal agitation **(Figure 2.28)**.
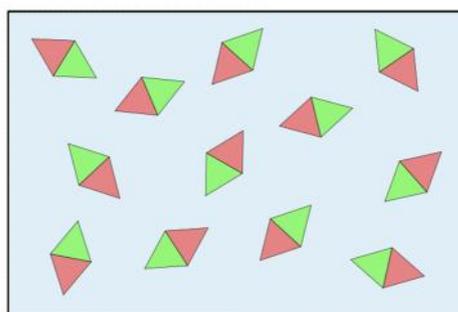
**Figure 2.28** Random orientation of magnetic moments in paramagnetic materials

In a short-ranged, the individual spins often interact with neighbouring spins in a cooperative fashion, where the direction of one spin influences the directions of its neighbouring spins. However, in bulk, it can cause a long-range magnetic ordering in the absence of applied field below a certain critical temperature.

There are three basic types of bulk magnetic properties: ferromagnetism, antiferromagnetism and ferrimagnetism. Ferromagnetism is the strongest and most common type of magnetism. Ferromagnetic material has unpaired electrons. In the absence of an external magnetic field, its magnetic moments (dipoles) has a tendency to orient parallel to each other to maintain a lowered-energy state. As a result, the material exhibit spontaneous magnetization (a net magnetic moment) as shown in **Figure 2.29**.
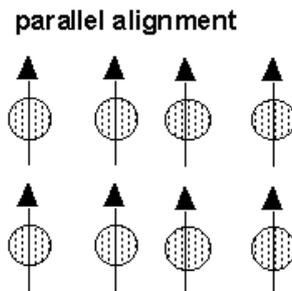

Figure 2.29 Parallel alignment of magnetic moment in ferromagnetic materials

Above the Curie temperature, T_C (a constant for every ferromagnetic substance), the electrons in the bonds are unable to keep the dipole moments aligned (due to the violent thermal motion), causing the material to lose its ferromagnetic properties and changes into a paramagnetic material.

In an antiferromagnetic material, the intrinsic magnetic moments of neighbouring valence electrons are aligned in the opposite directions (anti-aligned) **(Figure 2.30)**, resulting in zero net magnetic moment. The antiferromagnetic properties exist at sufficiently low temperatures. Above the Néel temperature (T_N) the material is typically paramagnetic.
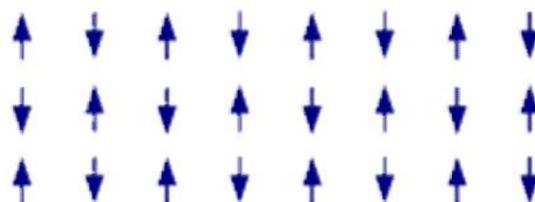

Figure 2.30 Alignment of magnetic moment in antiferromagnetic materials

Another type of magnetism is ferrimagnetism. In ferrimagnetic material, the magnetic moments of the atoms on different sublattices point in opposite directions (anti-aligned) as in antiferromagnetism. However, the opposing moments are unequal, **(Figure 2.31)** causing the spontaneous magnetization to remain. Thus, in the absence of magnetic field, ferrimagnets retain their magnetization. Above T_N (the main interaction in ferromagnetic materials are antiferromagnetic), ferrimagnets behave like paramagnets.
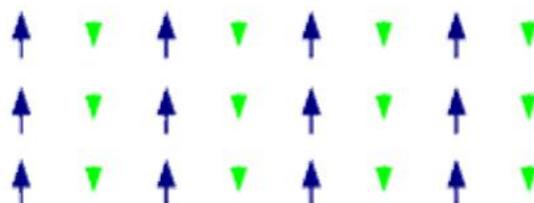

Figure 2.31 Alignment of magnetic moment in ferrimagnetic materials

The degree of magnetization of a material in response to an applied magnetic field is measured by its magnetic susceptibility, . The magnetic susceptibility value is commonly reported as molar susceptibility, $_M$:

$$\chi_M = \chi_g \times MW$$

where MW is the molecular weight, and the value of χ_g is directly obtained from the magnetosusceptometer. The molar susceptibility obtained has to be corrected for the inherent diamagnetic contribution from the ligands and metal ions using the Pascal's constants [34],

$$\chi_M^{corr} = \chi_M - \chi^{dia}$$

The χ_M^{corr} value is used to calculate the effective magnetic moment (μ_{eff}), which is then used to determine the magnetic properties, using the following relationship:

$$\mu_{eff} = 2.84 \; (\chi_M^{corr} T)$$

where T is the absolute temperature (in K). Sometimes, the equation is also presented as:

$$\mu_{\text{eff}} = 2.84 \left(_M{}^{\text{corr}} T - N \right)^{\frac{1}{2}}$$

where N is the temperature independence paramagnetism (TIP) of a metal ion. The value for each copper(II) ion is 60×10^{-6} c.g.s emu.

Theoretically, μ_{eff}, may be calculated from the following relationship:

$$\mu_{eff} = n(n+2)$$

where n is the number of unpaired electron(s).

Copper(II) ion $(3d^9)$ has one unpaired electron in the $3d$ orbitals. Thus, using the above equation, the calculated μ_{eff} value for mononuclear copper(II) complexes (at room temperature) is expected to be 1.73 B.M., while the value for dinuclear copper(II) complexes (two unpaired electrons) is 2.83 B.M.

Magnetic moments of copper(II) complexes can be classified into two main groups: (a) normal moments (1.8 – 2.0 B.M. for one unpaired electron), indicating the absence of any magnetic interaction between the unpaired electron of each copper(II) centre; and (b) magnetic moments smaller than the spin only value [35], also known as subnormal magnetic moments.

Copper(II) complexes with subnormal magnetic moments can be classified based on the type of mechanisms of magnetic interaction: (a) direct interaction; and (b) superexchange interaction. The direct copper-to-copper magnetic interaction is due to the direct bond between the two copper(II) ions, which is illustrated by copper(II) acetate monohydrate in which Cu-Cu distance is short, 2.64 A^o (μ_{eff}=1.43 B.M). For the second group, the copper-to-copper interaction is through the ligands, termed the super-exchange interaction [35,36].

Another important numerical value when discussing magnetic interaction is the 2J value (the exchange integral). It corresponds to the separation energy between a singlet and a triplet state [37]. For a dimeric copper(II) complex, the 2J value is calculated using the Bleaney-Bowers equation:

$$\chi_m = \frac{2g^2N\beta^2}{3\kappa T}(1+\frac{1}{3}e^{\frac{-2J}{\kappa T}})^{-1} + 2N\alpha$$

This equation is simplified by rearranging the above equation and by putting the values for all the constants [38]:

$$-2J = \{\ln[\{1.2186 \times 10^{-2}/(\chi_m - 0.12 \times 10^{-3})\} - 3]\}207.11$$

A negative 2J value indicates a singlet ground state and hence an antiferromagnetic interaction, while a positive 2J value indicates a triplet ground state and hence a ferromagnetic interaction.

The expected 2J values for copper(II) carboxylates range from -100 cm^{-1} to -500 cm^{-1}. The higher (more negative) value indicates a stronger antiferromagnetic interaction [39,40].

2.11 Cyclic Voltammetry

Cyclic voltammetry (CV) is an electrochemical technique with the objective to study the redox behaviour of a complex. In CV, the potential of a working electrode is changed linearly with time, in the potential region where reduction or oxidation of the material being studied occurs. The direction of the linear sweep is then reversed, and the electrode reactions are detected. A plot of current at the working electrode versus the applied voltage gives a cyclic voltammogram.

CV experiments involve a three electrode system: (a) saturated calomel electrode as the reference electrode; (b) a glassy carbon electrode as the working electrode; and

(c) a platinum wire as the counter electrode. Tetrabutylammonium tetrafluoroborate (TBABF$_4$) of molarity about 10^{-3} M may be used as the surporting electrolyte to ensure the required conductive media

A redox process is reversible when an analyte is reduced and oxidised on a forward scan and is then reoxidised or rereduced in a predictable way on the return scan (**Figure 2.32**). For an ideal reversible system, the peak potential separation, E_p (E_{pc} – E_{pa}) would be 59 mV for a one-electron process, and about 30 mV for a two-electrons process.
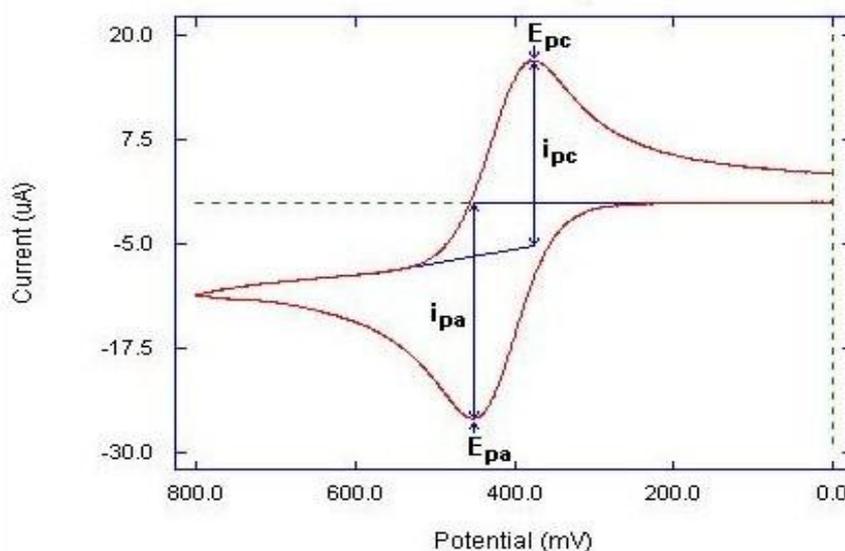

Figure 2.32 Cyclic voltammogram of a reversible process

For a reversible redox process, the peak currents ratio, I_{pa}/I_{pc} = 1 at all scan rates, and the peak current function i_p / $^{1/2}$ (= scan rate) is independent of . The peak current is given by the equation:

$$I_p = 2.69 \times 10^5 \, n^{3/2} ACD^{1/2} \, ^{1/2}$$

where *n* is the number of electron(s0 transferred/molecule, *A* is the electrode surface area (cm^2), *C* is the concentration (mol cm^{-3}), and *D* is the diffusion coefficient (cm^2 s^{-1}) [41].

Variation from the above parameters leads to a quasi-reversible process, which may be caused by the slow electron transfer kinetics and to the formation of chemical reaction following the electron transfer. In this case, the return wave could be observed but with amplitude less than the forward wave. It is characterized by the value of E_p greater than 59/n mV and the value of I_{pa}/I_{pc} of less than unity.

Most dimeric copper(II) carboxylates showed quasi-reversible redox processes [16,21,24,42] (which occur in a stepwise process) due to the change in the geometry of the coordination sphere. As one of the Cu(II) ion in the dimer is reduced to Cu(I), some structural distortion of the dimer took place [42] as Cu(II) ion prefers the square planar geometry while Cu(I) prefers the tetrahedral geometry.

References

[1]   A.M. Giroud-Godquin. *Coord. Chem. Rev*., 178, 1485 (1998).

[2]   R. Giménez, D.P. Lydon, J.L. Serrano. *Curr Opin Solid State Mater Sci*., 6, 527 (2002).

[3]   R.W. Date, E.F. Iglesias, K.E. Rowe, J.M. Elliott, D.W. Bruce. *Dalton Trans*., 1914 (2003).

[4]   D.W.Bruce, E. Lalinde, P. Styring, D. A. Dunmur and P.M. Maitlis, *J. Chem. Soc., Chem. Commun.*, 1986, 581; H.Adams, N.A. Bailey, D. W. Bruce, D.A Dunmur, E. Lalinde, M. Marcos, C. Ridgway, A.J Smith, P. Styring and P.M. Maitlis, *Liq. Cryst*., **2**, 381 (1987).

[5]   K. Ohta, O. Takenaka, H. Hasebe, Y. Morizumi, T. Fujimoto and I. Yamamoto, *Mol. Cryst., Liq. Cryst.*, 195, 135 (1991).

[6]   S. Chandrasekhar, B.K. Sadashiva and K.A. Suresh, *Pranama* 9, 471-480 (1977).

[7]   Fabio D. Cukiernik, Mohammed Ibn-Elhaj, Zulema D. Chaia, Jean-Claude Marchon, Anne-Marie Giroud-Godquin, Daniel Guillon, Antoine Skoulios, and Pascale Maldivi, *Chem. Mater.* 10, 83-91 (1998).

[8]   Van Niekerk, J. N., and Schoening, F. R. L., *Acta Cryst.*, 6, 227 (1953).

[9]   J. A. R. Cheda, M. V. Garcia, M. I. Redondo, S. Gargani and P. Ferloni, *Liquid Crystals*, Vol., No., 1, 1-14 (2004).

[10]   Tom Welton (Eds.), *Coordination Chemistry Review* 248 2459-2477 (2004).

[11]   Harry D. Pratt III, Alyssa J. Rose, Chad L. Staiger, David Ingersoll and Travis M, Anderson, *Dalton Trans*. 40, 11396 (2011).

[12]   M. Brett Meredith, C. Heather McMillen, Jonathan T. Goodman and Timothy P. Hanusa, *Polyhedron*, 28, 2355-2358 (2009).

[13]   Bojan Kozlevcar and Primož Šegedin, *Croatica Chemica Acta*, CCACAA 81 (2) 369-379 (2008).

[14]   http://en.wikipedia.org/wiki/Coordination_compound

[15]   Frank P. W. Agterberg, Hajo A. J. Provo Kluit, Willem L. Driessen, Henk Oevering, Wim Buijs, Miles T. Lakin, Anthony L. Spek and Jan Reedijk, *Inorg. Chem.*, 36, 4321-4328 (1997).

[16]   M. I. Mohamadin, N. Abdullah, *Cent. Eur. J. Chem.* 8(5), 1090-1096 (2010)

[17]   http://en.wikipedia.org/wiki/Aldol_reaction.

[18]   B. Adhikary, A. K. Biswas and K. Nag, *Polyhedron*, 6(6), 3208 (1987).

[19]   Pavia, Lampman, Kriz, *Introduction to Spectroscopy*, 3rd. Edition.

[20]   G. B. Deacon, R. J. Philips, *Coord. Chem. Rev.*, 33, 227 (1980).

[21]   Angel Garcio-Raso, Juan J. Fiol, Adela Lopez-Zafra, Jose A. Castro, Araceli Cabrero, Ignasi Mata an Elies Molins, Polyhedron, 22, 403 (2003).

[22]   P.Kogerler, P.A.M. Williams, B.S. Parajon-Costa, E.J.Baran, L.Lezama, T.Rojo, A.Muller, *Inorganica Chimica Acta*, 268, 239-248 (1998).

[23] C. Yenikaya, M. Poyraz, M. Sari, F. Demirci, H. Ilkimen, O. Buyukgungor, *Polyhedron,* 28, 3526-3532 (2009).

[24] S. Karthikeyan, T. M. Rajendiran, R. Kannappan, R. Mahalakshmy, R. Venkatesan and P. Sambasiva Rao, *Proc. Indian Acad. Sci. (Chem. Sci.)*, Vol. 113, No. 4, 245-256 (2001).

[25] K. S. Bharati, S. Sreedaran, A. K. Rahiman, K. Rajesh, V. Narayanan, *Polyhedron*, 26, 3993 (2007).

[26] http://en.wikipedia.org/wiki/JahnTeller_effect

[27] A. Garcis-Raso, J.J. Fiol, F. Badenas, E. Lago, E. Mollins, *Polyhedron*, 20, 2877 (2001).

[28] B. K. Koo. Bull. *Korean Chem. Soc.*, 22(1), 113 (2001).

[29] E. Kokot, R. L. Martin, *Inorg. Chem.*, 3, 1306 (1964).

[30] M. Petric, I. Leban and P. Segedin, *Polyhedron* Vol. 14, No. 8, pp. 983-989 (1995).

[31] M. Pajtasova, D. Ondrusova, E. Jona, S. C. Jona, S. C. Mojumdar, S. L'alikova, T. Bazylakova, M. Gregor, *J. Therm Anal Calorim* 100, 769-777 (2010).

[32] *Images for liquid crystals images*, york.ac.uk; phys.kent.edu; dept.kent.edu; sciencewhizkids.blogspot.com; nanohedron.com; mc2.chalmers.se.

[33] J. C. Marchon, P. Maldivi, A. M. Giroud-Godquin, D. Guillon, A. Skoulios and D. P. Strommen, *Phil. Trans. R. Soc. Lond*. A 330, 109-116 (1990).

[34] Gordon A. Bain and John F. Berry, *Journal of Chemical Education,* Vol. 85, No. 4 (2008).

[35] Motomichi Inoue, Michihiko Kishita and Masaji Kubo, *Inorg. Chem.*, Vol. 3, No. 2, (1964).

[36] Michinobu Kato, Hans B. Jonassen and James C. Fanning, *Chem Rev.*, 64, 99 (1964).

[37]   Ahyan Elmali, *Turk J. Phy.,* 24, 667-672 (2000).

[38]   D.W. Bruce and D O'Hare, *Inorganic Materials* 2nd Edition, John Wiley and Sons, New York, p. 70 (1996).

[39]   Rocio Cejudo, Gloria Alzuet, Joaquin Borras, Malva Liu-Gonzalez, Francisco Sanz-Ruiz, *Polyhedron*, 21, 1057-1061 (2002).

[40]   L. Strinna Erre, G. Micera, P.Piu, F. Cariati and G. Ciani, *Inorg. Chem.* 24, 2297-2300 (1985)

[41]   www.basinc.com/mans/EC_epsilon/Techniques/CycVolt/cv_analysis.html.

[42]   M. I. Mohamadin and N. Abdullah, *International Journal of the Physical Sciences*, Vol. 6(8) (2011).